

CORRELATION BETWEEN SIMULATED, CALCULATED, AND MEASURED MODEL ROCKET FLIGHT

Mark Abate, Eswar Anandapadmanaban, Larry Bao, Siddharth Challani, Jason Gaughan,
Andrew Jiang, Abhishek Lingineni, Anish Vora, Christopher Yang, Dustin Zhao

Advisor: Robert Murawski
Assistant: Samuel E. Zorn

ABSTRACT

Rockets are central components to the furthering of space exploration and the advancement of human communication. In this project, rocketry was explored first theoretically and then experimentally in order to measure different variables and understand the effects of changing parameters on the flight of a model rocket. After the parameters of payload and total impulse were tested, the relationships between each factor and apogee were analyzed. Team Rocket began by deriving Tsiolkovsky's Rocket Equation and utilizing the *OpenRocket* software to simulate rocket launches and test the aforementioned parameters. Scholars then constructed and launched model rockets to try to replicate the simulation data experimentally. Both simulation and experimental data confirmed that there was a negative, nonlinear correlation between payload and apogee where an increase in payload led to a decrease in apogee which was modeled by an exponential equation. Experimental data also supported a positive, logarithmic correlation between engine impulse and apogee. Overall, researchers concluded that optimal height can be achieved by maximizing impulse and reducing the payload as much as possible while maintaining the center of gravity above the center of pressure.

INTRODUCTION AND HISTORICAL BACKGROUND

Today's advanced rockets have existed for just a fraction of the time that man has been firing self-propelled projectiles. Devices that could be classified as rockets in various forms have emerged in the world's historical record for approximately a millennium; the underlying principles and physical models of rocket flight have been known for significantly longer.

Over two thousand years ago, circa 400 B.C.E., Greek mathematician Archytas of Tarentum constructed a wooden pigeon suspended on a wire over a fire. The pigeon was filled with water and as the bird was heated, steam was forced through small apertures in the rear, causing the illusion of flight (1). Nearly three hundred years later, Greek engineer Hero of Alexandria created a device dubbed an aeolipile (Fig. 1) (1).

This mechanism featured a sphere on an axle over a heated bath. The supports of the sphere were hollow, which allowed steam to fill it. Pressurized steam was then forced out of the L-shaped pipes. The sphere spun as a result of the fundamental action-reaction principle that would be



Figure 1: Hero's aeolipile (1)

canonized more than fifteen hundred years later as Newton's Third Law (2). This action-reaction principle is the foundation of modern rocketry, and of all previous advances in the field.

The next notable advance in rocketry would not come for another two centuries. In China, alchemists worked tirelessly to combine perceived passive (*yin*) and active (*yang*) substances to create a youth drug (3). Eventually, they combined saltpeter, sulfur, and charcoal in proper proportions to form rudimentary gunpowder (2). This powder was the first instance of the chemical that would be refined into the black powder fuel that is standard in modern model rockets (2). In the twelfth century, the Chinese developed the first device that could justifiably be called a rocket. The *ti lao shu* (ground rat) was a self-propelled tube that shot along the ground and was used primarily to startle enemy troops in combat (3).

In 1687, Newton famously published his *Philosophiae Naturalis Principia Mathematica*, which among other things outlined the Third Law of Motion, demonstrated by Hero some eighteen hundred years earlier (2). This law would again be confirmed in 1720 with an experiment performed on a car outfitted with a steam-powered motor (1). Nothing noteworthy would happen in the field of rocketry for another two centuries.

In the early twentieth century, three men—Tsiolkovsky, Goddard, and Oberth—drastically furthered human understanding of rocketry. Tsiolkovsky discovered the equation which governs rocket-powered flight (2). Goddard performed many experiments with solid-fuel rockets in conjunction with meteorological surveys, but soon decided a liquid-fuel rocket would achieve higher altitudes much more efficiently (2). He additionally produced the first liquid-powered rocket (Fig. 2) (1).

Goddard also pioneered gyroscopic guidance systems, payload compartments for instruments, parachute recovery of instruments and rockets, and many other things which have earned him the name “Father of Modern Rocketry” (1). Oberth, the third pioneer, wrote extensively on the subject of rocketry. Because of his books, many amateur rocketry groups emerged around the world, developing into the model rocketry community that exists today (1).



Figure 2: Dr. Goddard posing with his liquid-fuel rocket (1)

World War II featured landmark developments in rocketry under the guidance of Wernher von Braun and his team of researchers (3). Moreover, it forced rockets once again into the position of military tools rather than scientific instruments. Following the war, the United States and Soviet Russia entered into the Cold War. The Cold War featured, as a critical component, the Space Race, which would compel the public's interest in rocketry for years to come (2).

From the Space Race came many important achievements, primarily in the formation of NASA and its Apollo space program. The Apollo missions combined elements that had already

been established—multi-staged rockets, liquid fuel, recoverable instruments—and combined them into the Saturn V rocket (Fig. 3) (2). The Saturn V was a vessel unmatched by anything else known to rocketry, ultimately proving powerful enough to carry several men to the moon and back.

The Apollo missions—all flown in Saturn V rockets—formed the pinnacle of modern rocketry. Although space exploration via rocketry has been deemphasized at the public level, several private enterprises and amateur rocketeers around the world have continued on the trail paved by Archytas, the alchemists of China, Newton, von Braun, and the Apollo missions. From the humble beginnings of Archytas’s pigeon, rocketry has made possible both commercial and scientific enterprises: from the vast network of communications satellites to the Hubble Space Telescope, from space tourism to the International Space Station.

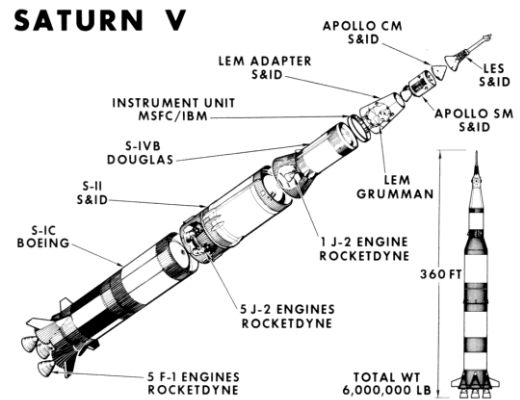


Fig. 3: The Saturn V rocket (2)

ELEMENTS OF THEORY

Mathematical Models of Rocket Trajectories

Tsiolkovsky’s Rocket Equation

One of the first mathematical models created to simulate the motion of rockets was formulated by Soviet scientist Konstantin Tsiolkovsky. A pioneer in what would eventually become astronautic theory, Tsiolkovsky first developed his equation in the idealistic setting of deep space, where external forces (i.e. aerodynamic drag and lift) do not exist. His equation was founded on the following idea: during a rocket’s flight, propellant from its thrust system is constantly ejected from the base of the rocket. The mass of the rocket, by consequence, is constantly changing throughout flight.

Consider a rocket of mass m traveling at velocity v at time t in deep space. The rocket emits a quantity of mass dm_e with ejection velocity v_e , producing a change in its momentum, dP .

Newton’s second law of motion relates the net force $\sum F_i$ to a change in momentum such that:

$$\sum F_i = \frac{dP}{dt} \tag{1.1}$$

where the change in momentum is equivalent to:

$$dP = ((m - dm_e)(v + dv) + dm_e(v + dv - v_e) - (mv)) \tag{1.2}$$

Solving yields:

$$dP = m dv - v_e dm_e \quad (1.3)$$

The exhaust mass is equivalent to the mass lost by the rocket. Then, using $dm_e = -dm$:

$$\sum F_i = m \frac{dv}{dt} + v_e \frac{dm}{dt} \quad (1.4)$$

In the theorized deep space setting, there are no external forces, and thus $\sum F_i = 0$:

$$-v_e \frac{dm}{dt} = m \frac{dv}{dt} \quad (1.5)$$

Integrating and further simplifying yields:

$$\Delta v = v_e \ln \left(\frac{m_o}{m} \right) \quad (1.6)$$

where m_o represents the initial mass of the rocket and fuel.

Tsiolkovsky's equation (1.6), however, is clearly flawed for practical circumstances regarding rocket motion and launch. The forces of gravity and aerodynamic drag have significant implications on the rocket's motion and flight path. Returning to Tsiolkovsky's original assumption (1.4) and then including weight and drag produces:

$$m \frac{dv}{dt} = -mg - \frac{1}{2} c_d \rho A v^2 + v_e \frac{dm}{dt} \quad (1.7)$$

where c_d represents the coefficient of drag, which is experimentally derived, ρ represents the density of the air, and A represents the cross sectional area of the rocket.

Developments in Gravitational Forces

Although a closed form solution cannot be directly developed from equation (1.7) without the use of technology, this formula permits an appropriate model of the rocket's motion, with the inclusion of real-world conditions.

In order to better model the rocket flight, the gravitational components must be accounted for in Tsiolkovsky's equation (1.6):

$$\Delta v = v_e \ln \left(\frac{m_o}{m} \right) - gt \quad (2.1)$$

Assuming that the mass in relation to time is a linear function, let $m = m_o - Rt$ where R is defined as the change of mass in relation to the change in time and is experimentally equivalent to 3 grams per 0.7 seconds for an Estes A8-3 rocket. Simplifying:

$$v(t) = -v_e \ln\left(1 - \frac{Rt}{m_o}\right) - gt \quad (2.2)$$

Then, integrating from $t = 0$ to the burnout time $t = t_b$:

$$y(t) = \frac{v_e m_o}{R} + \frac{v_e(m_o - Rt)}{R} \ln\left(\frac{m_o}{m_o - Rt} + 1\right) - \frac{gt^2}{2} \quad (2.3)$$

Additional Developments in Drag Forces

However, while equation (2.3) does factor in the alterations due to the gravitational forces, it still does not account for the additional force of drag. Beginning with (1.7), we assume that the thrust, or $v_e \frac{dm}{dt}$, is constant, and that the mass, given by $m = m_o - Rt$, is approximately equal to m_o throughout the flight. Then, substituting m_o for m , separating the variables, and then integrating from the start of flight to the time of engine burnout:

$$\int_0^{v_b} \frac{m_o}{T - m_o g - \frac{1}{2} c_d \rho A v^2} dv = \int_0^{t_b} dt \quad (3.1)$$

Substituting constants $\alpha = \frac{1}{2} c_d \rho A$ and $\beta = T - m_o g$ and then simplifying:

$$\frac{\beta t_b}{m_o} \sqrt{\frac{\alpha}{\beta}} = \tanh^{-1}\left(v_b \sqrt{\frac{\alpha}{\beta}}\right) \quad (3.2)$$

Generalizing the equation by setting $t = t_b$ and $v(t) = v_b$, isolating $v(t)$, and integrating:

$$\int_0^{t_b} \sqrt{\frac{\beta}{\alpha}} \tanh\left(\frac{\beta t}{m_o} \sqrt{\frac{\alpha}{\beta}}\right) dt = \int_0^{t_b} v(t) dt \quad (3.3)$$

Simplifying forms a general approximation of the height traveled after t seconds of powered flight with constant thrust T :

$$y_1(t) = \frac{m_o}{\alpha} \ln\left(\cosh\left(\frac{\sqrt{\alpha\beta}}{m_o} t\right)\right) \quad (3.3)$$

Substituting the engine burnout time into this equation gives the height of the rocket when it has run out of fuel. To find the apogee of the rocket, an equation for motion in which the rocket moves only under the influence of gravity and air resistance must be generated, given by:

$$m_o \frac{dv}{dt} = -m_o g - \alpha v^2 \quad (3.4)$$

Separating variables and integrating again, with integral bounds of the burnout event to the apogee event:

$$\int_{v_b}^0 \frac{m_o dv}{-m_o g - \alpha v^2} = \int_{t_b}^{t_a} dt \quad (3.5)$$

Simplifying and rearranging the integral expressions produces the time after launch at which the rocket reaches apogee:

$$t_a = t_b + \sqrt{\frac{m_o}{g\alpha}} \arctan \left(\sqrt{\frac{\alpha}{m_o g}} v_b \right) \quad (3.6)$$

Developing a Closed-Form Expression for the Apogee

Continuing with the derivation of the time of the apogee point, the equation can be further manipulated to derive a formula for the height traveled by the rocket to apogee. Substituting the burnout velocity v_b from (3.2), finding an expression for the height of the rocket as a function of time, and then replacing the time of apogee will produce a calculation of the desired apogee. Generalizing the integral bounds from (3.5):

$$t - t_b = \sqrt{\frac{m_o}{g\alpha}} \arctan \left(\sqrt{\frac{\alpha}{m_o g}} v' \right) \Bigg|_{v' = v_b}^{v' = v(t)} \quad (4.1)$$

Isolating $v(t)$ while substituting t_a from (3.6):

$$v(t) = \sqrt{\frac{m_o g}{\alpha}} \tan \left(\sqrt{\frac{g\alpha}{m_o}} (t_a - t) \right) \quad (4.2)$$

Integrating this with respect to time and simplifying produces a final equation for the apogee of the rocket, defined as $y(t_a)$ to distinguish it from the function $y_1(t)$ deduced earlier for the powered segment of flight. Notice that $y_1(t_b)$, the height of the rocket at burnout, is referring to this derived function for powered flight.

$$y(t_a) = y_1(t_b) - \frac{m_o}{\alpha} \ln \left(\cos \left(\sqrt{\frac{g\alpha}{m_o}} (t_a - t_b) \right) \right) \quad (4.3)$$

Substituting the previously derived expressions for t_a , v_b , and $y_1(t_b)$ forms a general equation for the apogee of a rocket flying under the influence of gravity and air resistance in terms of the defined constants:

$$y(t_a) = \frac{m_o}{\alpha} \ln \left(\cosh \left(\frac{\sqrt{\alpha\beta}}{m_o} t_b \right) \sqrt{1 + \frac{\beta}{m_o g} \tanh^2 \left(\frac{\sqrt{\alpha\beta}}{m_o} t_b \right)} \right) \quad (4.4)$$

Aerodynamics and Stability

Aerodynamics is the study of the motion of air especially with respect to moving or flying objects. Optimizing aerodynamics is crucial to the success of a model rocket. There are four forces acting on the model rocket: thrust—the force caused by the engine to move the rocket forward, weight—the gravitational force acting on the mass of the rocket, lift—the restoring force that stabilizes the rocket and helps control the motion of the flight, and drag—the aerodynamic force acting parallel to the relative wind (4).

In model rocketry, there are two key points: the center of pressure and the center of gravity. The center of pressure is the point where all forces of pressure seem to be concentrated and where the drag and lift act upon. Weight and thrust act on the center of gravity, where all of the mass seems to be concentrated. The thrust pushes the rocket upward in its motion while the weight and drag act antiparallel to the direction of motion. The lift pushes the rocket in the direction of the wind for stabilization (4). In figure 4, the center of pressure is located below the center of gravity. Such a positioning is ideal for a model rocket.

In the flight of a model rocket, it is crucial to control thrust and lift while minimizing drag. This could be easily done on the Alpha-type model rockets. These rockets had balsa wood fins, which made the drag easily manipulable through sanding and curving the fins. The Alpha fins were progressively sanded to have rounded edges, which are more aerodynamic. This made it easier for the wind to flow along the edge of the fin, giving the rocket less drag. The rocket was stabilized by the position of the center of pressure. In the rocket which partook in the mass variation study, the center of pressure was located at 19.05 centimeters below the tip of the nose cone. The center of gravity was at 18.10 centimeters below the nose cone tip, without accounting for the mass of an engine. According to Bernoulli's principle, flowing fluid (i.e. air) travels faster along certain areas like the fins. The air pressure is thus reduced in these areas and causes the force of lift. Additionally, when a gust of wind blows horizontally, the rocket tips slightly. The fins have a larger surface area than the rest of the rocket and thus, the nose tips

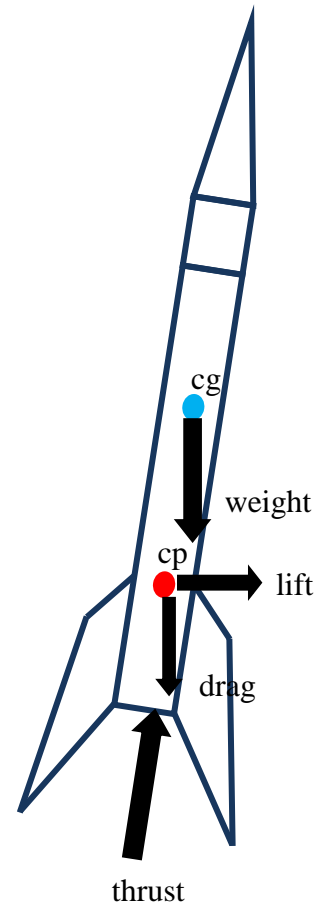


Figure 4: Four forces acting on a rocket in flight shown by arrows. The blue circle is the center of gravity. The red circle is center of pressure (adapted from (1))

against the wind. The lift however restores this because it tips the nose in the direction of the wind. Figure 5 shows how the lift affects the overall motion of the model rocket. If the lift and wind cancel each other out, the rocket will maintain a stable and neutral path. The restorative force can also make the rocket maintain an oscillation when the lift restores the shifts from the wind's gusts. The final motion is unstable when the lift fails to stabilize the rocket or it destabilizes the rocket. This also occurs when the center of pressure is above the center of gravity. The center of gravity acts like a pivoting point and when the lift acts on the rocket rather than turning it slightly, it would flip the rocket.

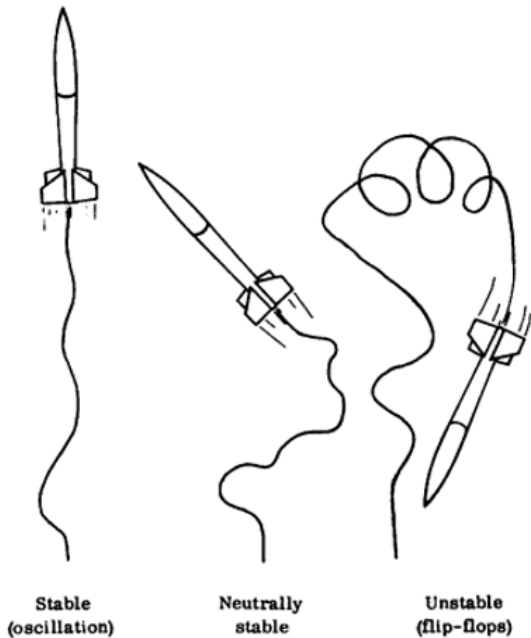


Figure 5: Possible model rocket flights representing stability. These three paths are caused by differences in lift, wind, and center of pressure and gravity (4).

An interesting phenomenon with the center of gravity is that it shifts during rocket flight (4). The center of pressure, dependent on the surface and shape of the rocket, remains the same throughout the flight. The center of gravity changes as the mass changes in the rocket. Each engine induces a different center of gravity. The different engines vary in the amount of propellant they have and also the amount of mass. During flight, the propellant is used up and the parachute deploys. This deploying of the chute also decreases mass. The nose cone pops off, the chute is released, wadding is ejected, and altimeter is also pushed out in certain cases. Through one flight, the center of gravity changes a tremendous amount because the engine and altimeter weigh more than the rocket body itself. By using larger engines, the stability changes much more through the course of a flight.

In modern rockets, various systems have been developed to control the stability of the rockets (5). Movable fins at the rear of the rocket are one form of this control. As the fins move and rotate, a torque is created around the center of gravity. This rotation allows for a steady oscillation in times of turbulence. Another form of stability is a gimbaled system, through which the exhaust nozzle can be turned. The thrust can be moved accordingly to the position of the center of gravity. Older rockets had additional rockets—known as vernier rockets—which would also generate torque around the rocket. Although model rockets do not have these mechanisms, it is interesting to note some of the methods used to control stability (6).

Computer Simulation

The open-source program *OpenRocket* by Sampo Niskanen (7) was used in this experiment to simulate rocket launches. The program required the parameters and dimensions of the parts, materials, and engines of a model rocket and output a simulation of the rocket in flight under ideal conditions.

The software modeled the four phases of rocket flight (Fig. 6). The first phase is the launch, during which the engine is ignited and the rocket is launched from the ground. Then, the rocket experiences powered flight. In this phase, the motor continues to power and accelerate the rocket. Next, the rocket enters coasting flight and glides without engine power until it reaches apogee. Finally, the recovery phase is the period in which the nose cone pops off and the parachute is deployed. The rocket then descends slowly and safely to the ground.

Because the software accounted for these four phases, it provided a graph of altitude versus time, which could then be compared to the experimental data collected. It also gave ballpark estimates of the maximum height (apogee) and how long it would take to reach.

Using the parameters of rockets in the *OpenRocket* software, the experimental launches were simulated. The major factors implemented during the real-world trials were accounted for in the models.

The software allowed for modifications of the relative positions of various parts, and it displayed the location of the rocket's center of gravity and center of pressure. *OpenRocket* also simulated the flights by going through the following process (7): first, the software initialized the rocket at a known position and orientation at time $t = 0$. Next, it computed factors such as wind velocity, turbulence, airspeed, launch angle, wind direction, drag, motor thrust, and gravitational forces on the flight of the rocket. Then, moments of inertia and the mass of the rocket were used to calculate the linear and rotational acceleration of the rocket. Finally, the program integrated the equations of motion for the rocket's position and orientation during a time step Δt and added this to the current time as such: $t + \Delta t$.

One of the major variables tested during the experimental stage was the effect of mass on the model rockets' apogee and flight. This was modeled by Niskanen's software by adding a variable mass component to the body tube of the rocket. It was important to contain the majority of the mass to a central position located at the front of the body tube for balance, and the additional mass was added in this area during the actual field experiments.

On *OpenRocket*, establishing a new configuration with a constant A8-3 Estes engine and altering the mass component by set intervals produced the following graph:

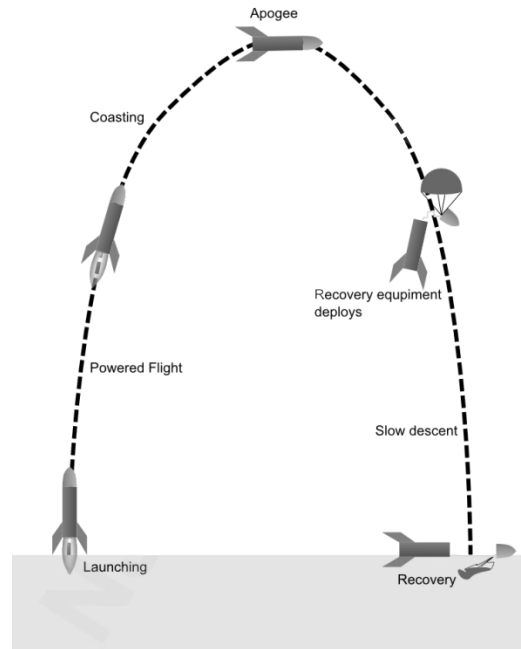


Figure 6: This is a diagram of an ideal model rocket flight, showing the various stages of rocket flight: powered flight, coasting flight, apogee, and recovery. This was created by Team Rocket on Inkscape (adapted from (8))

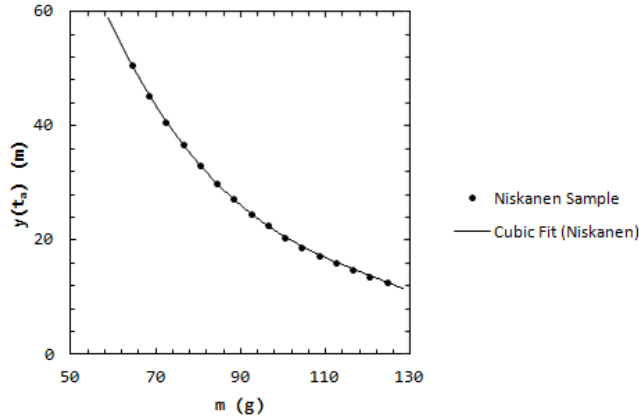


Figure 7: This graph shows simulated apogee as a function of rocket mass, showing a negative cubic regression. The data were taken from simulations on *OpenRocket* software. The graph was created by Team Rocket on Microsoft Excel.

Figure 7 shows a negative association between the total rocket mass and the apogee of the rocket flight. The best-fit line shows a large coefficient of determination with a cubic fit. In addition, the lack of outliers demonstrates the relative strength of the relationship between the explanatory and response variables. The form of the distribution is curved convexly, but it is generally clear that larger masses will result in reduced flight apogees and that smaller masses will allow the rocket to reach higher heights.

In addition to observing the effect of mass on apogee, the effect of mass on acceleration was studied by analyzing frames in videos of the launches. The *FBRD* was launched four times with varied masses. The model rocket was launched first with no added mass (total mass of 56.29 grams), then with an additional 10.56 grams, then with 20.46 grams more, and finally with an added 30.34 grams. Each of these launches was recorded using a high resolution camera with a frame rate of 24 frames per second. A custom meter stick was created in Autodesk Inventor Professional and Microsoft Paint, scaled based on a meter stick in the video, and then edited into each of the frames of the video. Then, starting from the beginning of the rocket's liftoff, the rocket's position in each later frame was recorded. These data points were then plotted and fitted to a third-degree polynomial. The data show that the heavier the rocket, the shallower the curve of its position-time graph (Fig. 8). This demonstrates that successively adding mass to rockets will consistently decrease the initial launch acceleration.

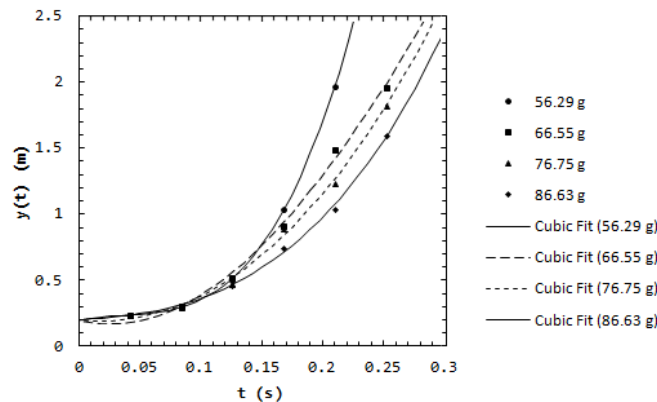


Figure 8: This graph shows height reached as a function of time, meant to show acceleration, showing a positive cubic regression. The experimental data was analyzed via video editing software. The graph was created by Team Rocket on Microsoft Excel.

Another parameter that could be modeled using *OpenRocket* was the model of engine used during the launch. The Estes engines differ in three main features, characterized by the classification of the model rocket engine. For example, an Estes A8-3 rocket has an average thrust of 8 Newtons with a 3 second firing delay. The “A” in the rocket name refers to the strength of the impulse; an “A” engine has an impulse of 2.5 Newton-seconds, and each subsequent letter type has a doubled impulse (e.g. a “C” engine has an impulse four times as strong as an “A” engine). These parameters can also dramatically affect the flight patterns of the model rockets, which can also be simulated by the *OpenRocket* software. Continuing with Niskanen’s sample model rocket, the effects of various changes on the apogee were examined:

Engine Type	Specifications	Equation (4.4) Apogee (m)	<i>OpenRocket</i> Apogee (m)
A	8-3	58.66	69.80
B	6-4	152.62	172.0
C	6-5	271.89	320.0

Figure 9: This table shows apogee by engine type, using *OpenRocket* simulations and Equation 4.4. The table was created by Team Rocket on Microsoft Word.

Figure 9 shows that, in both *OpenRocket* simulations and calculations of equation (4.4), any increases in impulse are associated with significant increases in apogee. In fact, the increase from “A” (2.5 N-s) engines to “B” (5 N-s) engines caused the apogee to more than double in both the simulation and the equation. For all three engines, the equation apogee was less than the corresponding apogee in the *OpenRocket* simulation. This is because the simulations on *OpenRocket* use a different method of predicting apogee than equation (4.4).

EXPERIMENTAL DESIGN

The *OpenRocket* simulations were used to test the parameters affecting rocket flight. The aspects of the Estes model rockets were measured and varied in the software parameters. With these quantifications, *OpenRocket* estimated the apogees of the specific rocket designs; these estimates were then compared to observed measurements during experimental launch.

There were three different models of rockets used in the experiment. Despite the slight differences in parameters such as number and composition of fins, diameter, and length, each model met certain basic requirements. Each was comprised of a removable polystyrene nose cone, a primary cardboard body tube, and a cardboard inner tube containing the engine. The solid propellant in each engine was black gunpowder. Fins were made of smooth cardboard, polystyrene, or balsa wood. There were three models of rockets used: the Generic E2X, the Viking, and the Alpha. The Generic E2X rockets used preassembled sets of four trapezoidal fins and were the largest of the three models. The Viking rockets had up to five cardstock fins that were easily customizable, but needed to be attached with glue. The Alpha rockets had three balsa wood fins that could easily be sanded to add curvature. Each rocket also had an engine block to prevent the engine from moving during launch, a rubber shock cord to attach the nose cone to the body tube, a launch lug through which the metal rod of the launch pad was threaded, and a plastic parachute or streamer to prevent damage to the rocket during recovery.

After the construction and simulation of the model rockets, preparations for launch were made in an open field. The longest diagonal on the field was measured and the launch equipment

was placed at its midpoint. A launch pad was set up at this midpoint with observers stationed at the ends of the diagonal. Their tasks were to measure the angle of elevation of the rocket at apogee with AltiTrak angle-measuring devices; these angles were used in combination with the distance of the observer from the rocket to calculate the apogee. The launch pad had a metal rod which was threaded through the launch lug of the rockets to provide a more vertical launch. Parallel to this metal launch rod, a two-meter stick was set up. Two or three timers measured the time taken to reach apogee to the nearest hundredth of a second.

To launch the rockets, an engine was inserted into the inner tube through the bottom with the nozzle facing outwards. An altimeter, which measures height in comparison to relative air pressure, was inserted through the top of the rocket, behind the nose cone to measure apogee. Each rocket had three $\frac{1}{8}$ inch holes drilled into the body to facilitate the measurement of pressure. Wadding, made of thin paper, was also inserted into the rocket above the engine to prevent heat damage to the altimeter and body tube. An igniter was inserted into the engine and connected to a launch controller. Then, the metal rod was threaded through the launch lug and the rocket was placed on the launch pad. Finally, the fuse was ignited from several meters away using a launch controller. The operation of the engine allowed the flight of the rocket to be separated into four phases as described earlier. By analyzing individual frames from the video recording of the launch, the acceleration at liftoff was calculated using the two-meter stick as a reference for distance and individual frames as a reference for time.

RESULTS AND ANALYSIS

Variation of Rocket Mass

One aspect of this study was to experimentally determine the effects of the rocket's mass on its apogee. Two different model rockets were each launched four times with different masses added to each flight. The masses were added to the rocket by lead shots, which were placed within the hollow nose cone. Lighter weights—ranging from zero to ten grams—were added to one rocket, and heavier ones—up to thirty grams—were added to another. As the compositions of the rockets were not entirely similar, the two data sets were examined separately. The first model rocket examined, *The Firefly*, produced the progression as seen in Figure 10.

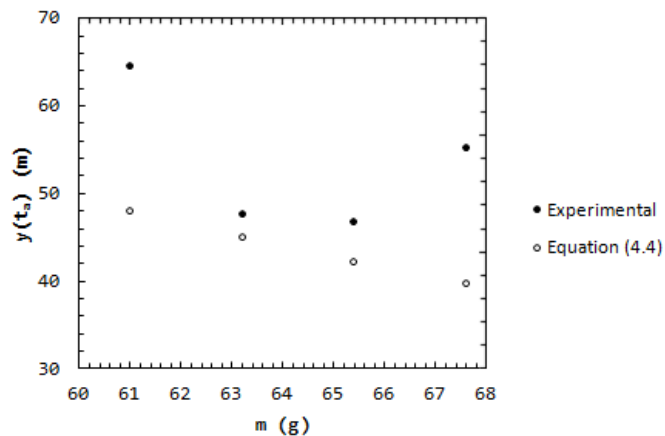


Fig 10: Apogee vs. Lighter Masses. This graph shows the trend in lighter masses. Also can be seen is the comparison with theoretical predictions. The theoretical equation under predicts the apogees.

The expected points come from calculations made using equation (4.4) with the dimensions of *The Firefly* and data from *ThrustCurve.org* (9). In this case the expected points follow a widely different trend than the general trend of the data. Error in this regard was expected due to the simplifying assumptions made in deriving equation (4.4); however it is not clear that the wide variation between the data and the expected points can be entirely explained by these approximations. In addition to contradicting the *OpenRocket* simulation based on mass and the results of equation (4.4), these initial results of the variation of mass were inconclusive. While it was expected for the apogee to continuously decrease as more mass was added, there were several possible experimental errors that may have affected the data. The rightmost point (67.6, 55.33) may be a result of these errors; the probable outlier lies out of the general trend of the graph, and makes the overall strength of the scatterplot relatively weak. Another possible source of error is a technical difficulty that was encountered; during the fourth launch of the *Firefly*, the ejection charge of the engine caused the shock cord to snap, allowing the recovery system with the altimeter to be launched significantly higher than the apogee of the *Firefly*. This would have caused a higher-than-accurate measured apogee on the altimeter.

In order to more closely examine the effects of mass on the apogee, the team conducted another study by launching a different rocket, the *FBRD*. Over four launches, lead shot was added to the nose cone of the *FBRD* to increase its mass by increments of ten grams. The progression is plotted in figure 11. The experimental, simulated, and theoretical are plotted in figure 11 and noted in figure 12. From figure 12, it can be seen that the theoretical predictions are much closer to the experimental than are the simulated.

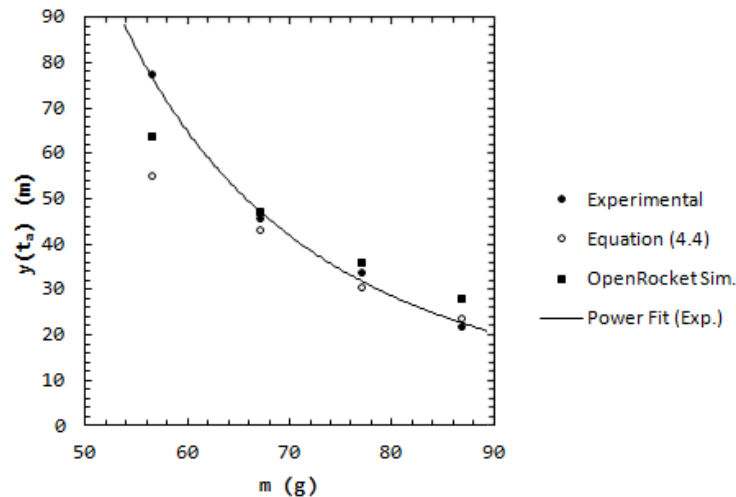


Fig. 11: Apogee as a function of rocket mass. The experimental, theoretical and, simulated points are plotted.

These data are more consistent with what the simulation and equation (4.4) predict for the apogee as a function of mass. With lighter masses, external sources of error (e.g. wind) had a much greater effect on the data, but the heavier masses lessened the effects of these factors, thus yielding more fitting data. These data therefore show that while the addition of mass stabilizes rocket flight and makes it less susceptible to external factors, increasing mass generally decreases apogee. Thus, rocket scientists must find a delicate balance for mass in that a rocket must be heavy enough for stable flight, but light enough to reach the intended apogee. The fit shows that greater mass decreases the apogee. The negative non-linear association roughly

follows the trend predicted by equation (4.4), though the data are clearly offset to some degree from these expected values. This offset can likely be explained by the simplifying assumptions made in deriving equation (4.4) but is not large enough to suggest an entire inconsistency between our observations and predictions.

Mass (g)	Experimental Apogee (m)	Equation (4.4) Apogee (m)	<i>OpenRocket</i> Apogee (m)
56.29	77.87	55.30	64.20
66.85	46.26	41.30	47.20
76.75	34.23	30.89	36.40
86.63	22.13	23.86	28.40

Fig. 12: Comparison of experimental, theoretical, and simulated apogees. This chart compares the field results with predicted results, showing the accuracy of these measures.

The overall study of mass versus apogee showed that the two variables—explanatory and response—have a negative association under ideal conditions. While there were exceptions in specific circumstances when the external forces overruled the addition of mass, the general trend between was clear. Moreover, we can observe explicit similarities between the simulation in Figure 7 and the above two graphs. Both the simulated data and collected data show that mass and apogee have an exponential relationship.

Variation of Engine Type

The study was further concerned with discerning how changing the engine specifications in a given rocket would affect its apogee. This aspect of rocket flight was investigated by considering the apogees reached by a single rocket launched using three different engine types: the A8-3, the B6-4, and the C6-3. The Alpha rocket *The Survivor* was used to gather the data. Each engine has its own specifications. Figure 13 shows a graph of theoretical expectations and experimental data for the apogee of the rocket as a function of engine impulse. The overall fit is logarithmic, with a positive association between the engine impulse and apogee.

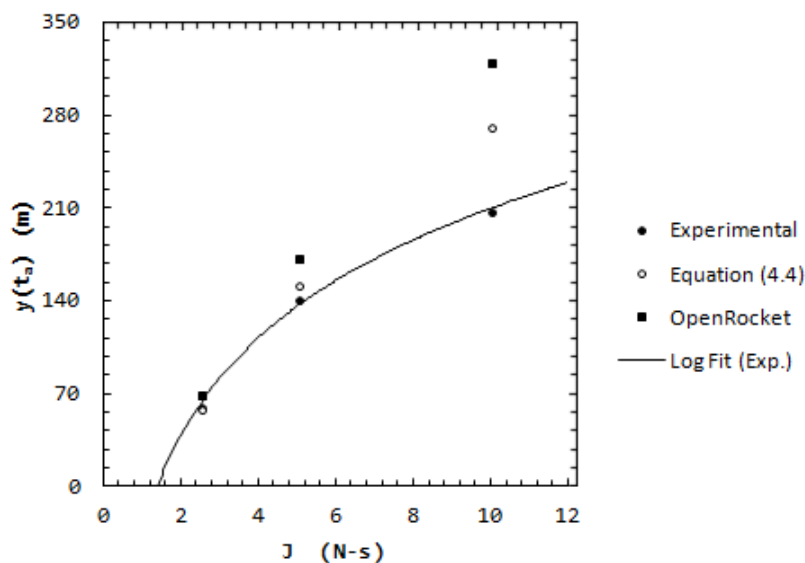


Fig. 13: Apogee as a function of impulse.

Plotting the impulse versus apogee data shows a non-linear, positively associated relationship. The least squares regression line for this graph is:

$$\hat{y} = 106.687 \ln x - 35.77$$

where \hat{y} represents the expected apogee values and x represents the strength of the impulse. The residual sum of squares for this regression analysis is 41.29, indicating a very good fit. With this regression line, predictions can be made for different types of engines that we did not use. Statistically, caution must be taken because of extrapolation beyond the range of the data points.

Predictions for Larger Engine Types

Engine Type	Impulse (N-s)	Apogee(m)
D	20	283.833
E	40	357.783
F	80	431.733
G	160	505.683

Figure 14: Predictions for Larger Engines—Impulse vs. Apogee

Figure 14 above shows predictions up to a G engine. This however does fail to account for various possible factors such as the changes in relationship beyond a certain engine size. Furthermore, as the engine itself gets larger, it will need a larger rocket. Thus these predictions can only be seen as a crude depiction of what may occur. The 20 N-s and 40 N-s approximations are much more reliable because of their proximity to the actual data set. However, the 80 and 160 N-s estimations may not be as accurate.

CONCLUSIONS

The goal of this experiment was to measure the effects of changing parameters on the flight patterns of a model rocket and to be able to use functions to accurately predict the extent of these effects on future launches. In addition to measuring the correlation of mass with both apogee and initial acceleration, the relationship between engine impulse and apogee was also explored. Rocket mass and apogee have a nonlinear, inverse relationship which can be modeled by an exponential function. In some cases, external forces such as wind overpowered the effects of mass; despite this, it is clear that increasing mass decreases apogee. Additionally, increasing the payload of the rocket decreases its initial acceleration. The position of a rocket with a given mass and engine type can be modeled by a cubic polynomial function, and engine type and apogee have a logarithmic relationship. Overall, it can be established that implementing engines with stronger impulses yields in higher launches. Therefore, to optimize apogee, scientists should construct rockets in a manner that minimizes mass yet maintains a distribution of mass such that the rocket remains stable in flight. Furthermore, it is evident that the most aerodynamic rocket designs must be both light and have an engine with a large impulse, which is in accordance with the derived rocket apogee equation.

REFERENCES

1. Benson T. Brief History of Rockets [Internet]. National Aeronautics and Space Administration ; [2014 Jun 12, cited 2014 Jul 28] . Available from: http://www.grc.nasa.gov/WWW/k-12/TRC/Rockets/history_of_rockets.html
2. Hartmann A. History of Rocketry [Internet]. Cape Canaveral(FL):Spaceline Inc.; cited 2014 Jul 28]. Available from: <http://www.spaceline.org/spaceline.html>
3. Stamp J. 2013. The History of Rocket Science: When was the First-Ever Rocket Built?. Smithsonian Magazine [Internet]. [cited 2014 Jul 28]. Available from: <http://www.smithsonianmag.com/innovation/the-history-of-rocket-science-4078981/?no-ist>
4. Barrowman J. 1970. Stability of a Model Rocket in Flight [Internet]. Phoenix(AZ):Centuri Engineering Company; [cited 2014 Jul 28] Available from: <http://www.rockets4schools.org/images/Rocket.Stability.Flight.pdf>
5. Benson T. Ideal Rocket Equation [Internet]. National Aeronautics and Space Administration ; [cited 2014 Jul 28] . Available from: <http://exploration.grc.nasa.gov/education/rocket/rktpow.html>
6. Benson T. Examples of Controls [Internet]. National Aeronautics and Space Administration; [cited 2014 Jul 28] . Available from: <http://exploration.grc.nasa.gov/education/rocket/rktcontrl.html>
7. Niskanen S. 2013. OpenRocket Technical Documentation. [Internet]. [cited 2014 Jul 28]. Available from: <http://openrocket.sourceforge.net/techdoc.pdf>
8. Senoski Walter E, inventors; Senoski Walter E, assignee. 1975 Sep 9. Model rocket and recovery device. United States patent US 3903801 A.
9. Coker J. 1998. Thrust Curve Hobby Rocket Motor Data [Internet]. [2014 Jul 25, cited 2014 Jul 31] . Available from: <http://www.thrustcurve.org>